JOURNAL OF CATALYSIS 118, 111–124 (1989)

CO Oxidation over Pt/γ-Al_2O_3 under High Pressure

EUGENE C. SU, WALTER G. ROTHSCHILD, AND H. C. YAO

Engineering and Research Staff, Ford Motor Company, Dearborn, Michigan 48121

Received March 23, 1987; revised October 25, 1988

The oxidation of CO over a Pt/γ-Al_2O_3 catalyst was studied by cyclic injection of CO and O_2 pulses under CO and O_2 pressures of 2 and 1 kPa, respectively, at temperatures of 330–650 K. A boundary reaction model yielded kinetic parameters in agreement with the results of published low-pressure studies. For CO_2 formation from $O_2(g)$ + $[CO]_{ad}$, CO desorption was the most important step and showed multipeak characteristics and a low activation energy (10 kJ/mol) for the boundary reaction was found. CO_2 formation from $O_2(g)$ + [CO] as well as from CO(g) + $[O]_{ad}$ resulted from boundary reaction at oxygen island. A reaction mechanism was proposed to account for the kinetics observed and interpret the varying observations noted in low-pressure studies in terms of diffusion-disguised kinetics.

I. INTRODUCTION

Since the pioneering work of Langmuir (*1*), the oxidation of CO over Pt, a model reaction amenable to fundamental analysis, has been the subject of numerous studies aimed at elucidating the reaction mechanism and quantifying its kinetic parameters. Review of the studies with low-index plane and polycrystalline Pt under low pressures ($\approx 10^{-4}$ Pa) (*2, 3*) has shown that dissociative adsorption of oxygen is essential and that the oxidation product, CO_2, forms mainly by the Langmuir–Hinshelwood (LH) mechanism, i.e., by an activated reaction of oxygen adatoms with adsorbed CO. While CO adsorption is reversible under oxidation conditions of interest, desorption of oxygen adatoms, by recombination, is negligible below 700 K and there does not appear to be any strong bonding of CO_2 on Pt. In addition, both the sticking coefficients for CO and O_2 adsorption show a strong coverage dependence. The LH pathway was inferred from studies showing energy barriers incompatible with the alternate Eley–Rideal (ER) mechanism; i.e., CO_2 forms by reaction of oxygen adatoms with CO molecules from the gas phase or in a weakly adsorbed state.

The high-pressure studies (*4*) dealt mostly with steady-state multiplicity and self-sustained oscillations of CO oxidation over Pt at atmospheric pressure. While theoretical studies of the reaction system predict unstable steady states under certain operating conditions, experimental investigations have shown that changes in surface morphology and hence activity (as a result of surface reconstruct), oxidation state of the metal, impurities in the metal or gas, catalyst pretreatment, and coverage-dependent activation energy all play a significant role. Several low-pressure studies of CO oxidation over Pt (*4, 5*) have reported similar unstable behavior.

The low-pressure kinetics has been employed to correlate high-pressure CO oxidation data (*6, 7*). Other high-pressure studies show that the oxidation rate is not linearly related to CO coverage on Pt (*8*) and that CO_2 formation relates to CO adsorbed linearly on Pt atoms sharing an oxygen atom with a Pt neighbor (*9*). Still other studies (*10, 11*) showed that high-pressure CO oxidation over Pt appears to follow both LH and ER pathways. These studies employed either slow instrument (*8, 9, 11*) or high temperature (*6, 7, 10*) and hence their results, though very illuminating, are

0021-9517/89 $3.00

insufficient to define the reaction mechanism of an extremely fast reaction. Thus, comprehensive studies are in order concerning whether the reaction mechanism and kinetic parameters found from low-pressure studies are applicable to the oxidation process under high pressures.

This paper presents the results from such a study of CO oxidation kinetics on a monolithic $Pt/\gamma\text{-}Al_2O_3$ catalyst at CO and O_2 pressures of 2 and 1 kPa, respectively, between 330–650 K. A cyclic pulse injection technique was employed to evaluate, in the time domain of $\approx$1 sec, the two reaction systems

$$CO(g) + [O]_{ad} \rightarrow CO_2$$

$$O_2(g) + [CO]_{ad} \rightarrow CO_2$$

The pulse injection technique was chosen because it would yield kinetic information not obtainable from a steady-state experiment, the latter being also prone to unstable behavior noted above.

II. EXPERIMENTAL

Catalyst sample. The Pt catalyst bed consisted of seven pieces of monolithic cordierite substrate (Corning), each coated in identical manner with $Pt/\gamma\text{-}Al_2O_3$. The catalyst sample was prepared by coating the channel walls of the substrate with a suspension of γ-alumina containing aqueous hexachloroplatinate in a manner to ensure Pt dispersion (*12*). X-ray diffraction and surface area determinations showed monolayer Pt dispersion over the alumina with a Pt loading of 1.1 μmol/m^2 BET (*12*).

The individual catalyst pieces were placed end to end in a Pyrex U-tube reactor that ensured a good fit to the contour of the monolithic substrate, the reactor being contained in a tube furnace with temperature control within 1 K. The catalyst section (8.4 cm long with a square cross section of 0.09 cm^2) was covered with aluminum foil to prevent direct exposure to thermal radiation.

Pulse injection. The apparatus and methods of pulse injection and gas analysis by mass spectroscopy were as described elsewhere (*13*). The pulse carrier gas consisted of ultrahigh purity helium (99.9999%) at a flow rate of 300 cm^3/min. A 3-cm^3 pulse of reactant gas, of either 2% CO or 1% O_2 in He at atmospheric pressure, was injected into the carrier gas stream after a fixed period of 18 sec had elapsed. The choice of this pulse interval was dictated by slow response due to transport and instrument dynamics and the choice of pulse volume and concentration by instrument sensitivity and catalyst activity.

The cyclic injection of CO and O_2 pulses was carried out as follows: a CO pulse was succeeded by an O_2 pulse which was, in turn, followed by another identical CO pulse and so on. Between the injections of each pulse, the carrier gas stream swept the reactor clean of the reactant gas in the gas phase.

This procedure allowed simultaneous evaluation of the CO_2 formation and the disappearance of each reactant gas for the two reaction systems under study. It also ensured that the initial condition prior to each pulse injection had reached a quasi-steady state, in the sense of being definable and hence amenable to meaningful analysis.

After constant oxidation had been reached, the amounts of the CO_2 evolution and of the reactant consumption were determined by the digitalized concentration profile of each component of interest. In addition, the effects of pulse interval and the maximum CO_2 formation by multiple pulse injection were determined.

III. DISCUSSION OF RESULTS

In this section we note the significant features of the experimental results of CO_2 formation by $O_2(g) + [CO]_{ad}$ during the O_2 pulse and by $CO(g) + [O]_{ad}$ during the CO pulse. A quantitative analysis of the reaction kinetics is given in Section IV and in Section V we discuss the reaction mechanisms underlying the kinetics found in this

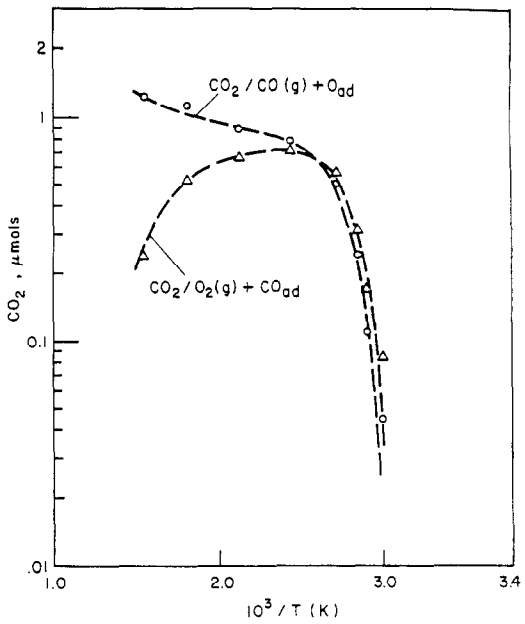

FIG. 1. Effect of temperature on CO_2 formation.

study in comparison with low-pressure kinetics reported in the literature.

(A) CO_2 Formed by $O_2(g)$ + $[CO]_{ad}$

Temperature effect. Figure 1 shows that CO_2 formation increases very rapidly with temperatures up to ≈400 K, leveling off thereafter with a rapid pace of descent above 500 K. This is characteristic of the crucial role of CO desorption in yielding sites for the adsorption of O_2, an essential step in the oxidation process. The descend at elevated temperatures results from the exponential increase of the desorption rate with temperature, i.e., CO_2 formation then becomes limited by the amount of adsorbed CO remaining.

The rising slope of the CO_2 evolution curves shown in Fig. 2A is a measure of the CO_2 formation rate. As shown, the CO_2 formation rate increases with temperature from 350 to 390 K. However, similar curves (not shown) indicate that the CO_2 formation rate above 400 K remains the same as observed at 390 K. This lack of temperature dependence suggests that only the CO_2 formed below 390 K are valuable for the study of reaction kinetics.

Pulse interval effect. Figure 4A shows that CO_2 formation increases with the length of pulse interval up to ≈370 K and begins to follow a reverse trend above 400 K. This results from CO desorption playing a decisive role as noted above. Though formation of less reactive precursor states of initially adsorbed CO can also lead to a dependence of CO_2 formation on the pulse interval (*14*), such an interpretation (*15*) is no longer commendable since a kinetic model (Section IV) including the CO desorption step fully explains the observed increase in CO_2 formation.

As shown in Table 1, it is the pulse interval after the CO pulse that affects CO_2 formation. Since adsorbed oxygen does not desorb under 700 K, the pulse interval after the O_2 pulse would not have any effect.

Multiple pulse experiment. The doublet injection experiment shows that appreciable CO_2 formed from the second O_2 pulse

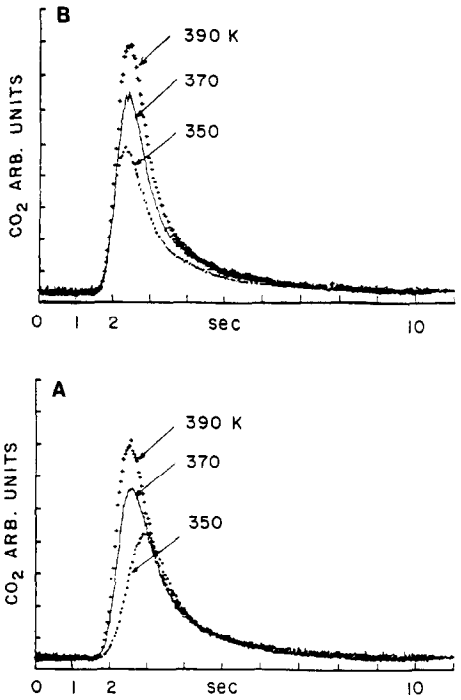

FIG. 2. Evolution of CO_2 after injection of (A) O_2 pulse and (B) CO pulse at 350, 370, and 390 K.

TABLE 1

Effect of Pulse Interval and Multiple Injection at 350 K

CO injection		O_2 injection		CO_2 formed (μmol)	
No. of pulses	Interval (sec)	No. of pulses	Interval (sec)	CO pulse	O_2 pulse
1	18	1	18	0.42	0.46
1	36	1	18	0.50	0.50
1	72	1	18	0.57	0.54
1	18	1	36	0.43	0.48
1	18	1	18	0.42	0.48
1st	18	1st	18	0.64	0.45
2nd	18	2nd	18	0.00	0.19

(Table 1). Quintuplet injection runs (not shown) indicate a negligible amount of CO_2 formed after the second pulse. Thus, the doublet experiment provides a good measure of the maximum active sites. The maximum active sites at temperatures above 400 K may be estimated from the CO_2 formed during injection of the CO pulse as noted below.

(*B*) CO_2 *Formed by* $CO(g) + [O]_{ad}$

Temperature effect. The rapid increase in CO_2 formation below 400 K (Fig. 1) results from the increased adsorption of O_2 on the sites vacated by CO_2 formation as well as by CO desorption. However, this increasing trend continued at elevated temperatures because CO desorption only enhances O_2 adsorption with a corresponding increase in CO_2 formed during the injection of the subsequent CO pulse.

Figure 2B shows that CO_2 formation is essentially independent of temperature. Moreover, as shown in Fig. 3B, the CO_2 evolution precedes the CO breakthrough, indicating complete oxidation of CO. Thus, the data do not warrant a quantitative evaluation of the reaction kinetics.

Pulse interval effect. Figure 4B shows a trend of increasing CO_2 with the lengthening of the pulse interval up to 400 K, as expected due to additional sites, vacated by CO desorption, available for O_2 adsorption. In contrast to the case of CO_2 formed during the O_2 pulse, pulse interval has no effect on CO_2 formed above 400 K, indicating fast oxidation of the CO on the metal followed by full oxygen coverage. Moreover, the CO_2 formed increases with temperature. We interpret this as to reflect multipeak CO desorption characteristics (*16–19*).

Multiple pulse injection. Table 1 shows complete removal of the adsorbed oxygen during the first CO pulse in a doublet injection run; this is also true in the case of the quintuplet injection run. This together with the pulse-interval independence noted above indicates that the CO_2 formation during the CO pulse provides a quantitative measure of the maximum active sites above 400 K.

IV. DATA CORRELATION

The pulse evolution curves (such as shown in Figs. 2 and 3) can be used for the evaluation of relatively simple reaction kinetics, after deconvolution to isolate the kinetic components from the extraneous time

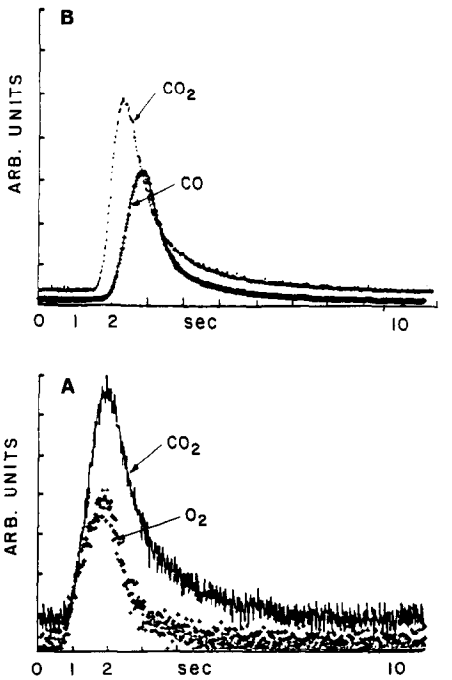

FIG. 3. Evolution of CO_2 and of (A) O_2 after injection of O_2 pulse and (B) CO after injection of CO pulse at 350 K.

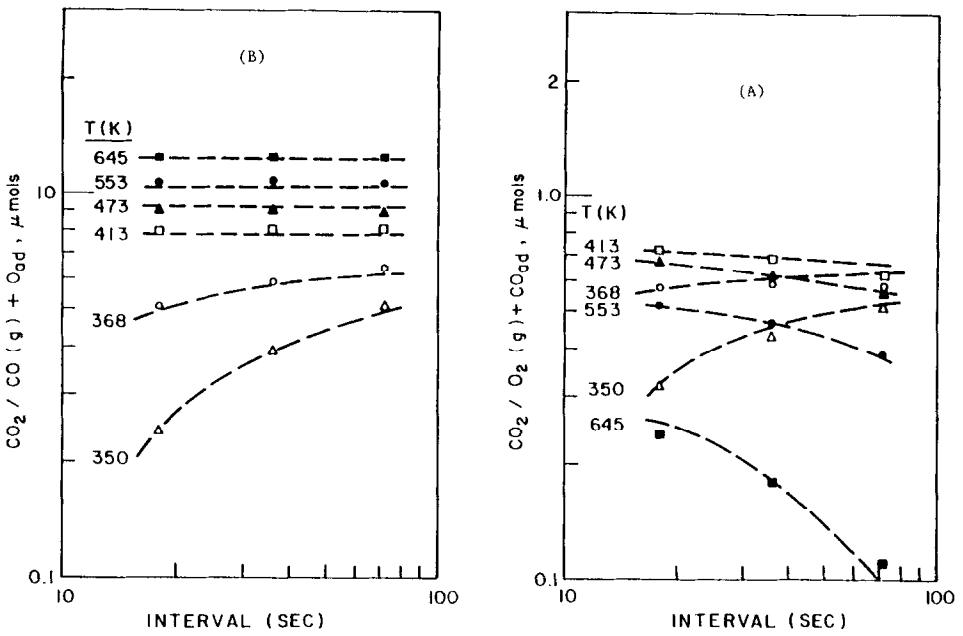

FIG. 4. Effect of pulse interval on (A) $CO_2/O_2(g)$ + $[CO]_{ad}$ and (B) $CO_2/CO(g)$ + $[O]_{ad}$.

constants due to transport and instrument dynamics. Such an attempt was not made in view of the dominance of the extraneous time constants, as indicated by a long-tail decay, whereas the pulse passed the catalyst bed in $\approx$1 sec. A mathematical model such as described below is necessary for a rigorous quantitative analysis. The kinetic model used in this analysis took into account the following reactions:

$$CO(g) + S \rightarrow [CO]_{ad} \quad (1.1)$$

$$[CO]_{ad} \rightarrow CO(g) + S \quad (1.2)$$

$$[CO]_{ad} + [O]_{ad} \rightarrow CO_2 + 2S \quad (1.3)$$

$$O_2(g) + 2S \rightarrow 2[O]_{ad} \quad (2.1)$$

$$[O]_{ad} + [CO]_{ad} \rightarrow CO_2 + 2S \quad (2.3)$$

Reactions (1.1) and (1.2) denote, respectively, the adsorption and desorption of CO on active sites (S). Reaction (2.1) for the dissociative adsorption of oxygen assumes a single step to represent the overall process of reversible adsorption of O_2 followed by dissociation in the presence of paired adjacent sites. Reactions (1.3) and (2.3) prescribe the CO_2 formation reactions in the presence of preadsorbed oxygen and CO, respectively. The desorption of oxygen adatoms by recombination—reaction (2.2) not shown—is negligible over the temperatures studied.

On the basis of the findings of low-pressure studies, the following rate expressions $R(i, j)$ for reactions (i, j) were derived,

$$R(1, 1) = k(1, 1) * \{1 - \theta(CO) - \theta(O)\} * P_{CO} \quad (3a)$$

$$R(1, 2) = k(1, 2) * \theta(CO) * \exp\{\beta(T) * \theta(CO)\} \quad (3b)$$

$$R(1, 3) = k(1, 3) * \theta(CO) * \theta(O)^{0.5} \quad (3c)$$

$$R(2, 1) = k(2, 1) * P_{O2} * \{1 - \theta(CO) - \theta(O)\}^{2.0} \quad (4a)$$

$$R(2, 3) = k(2, 3) * \theta(CO) * \theta(O)^{\alpha}, \quad (4b)$$

where $k(i, j)$ is the rate constant for reactions (i, j) and is equal to $k_0(i, j) * \exp\{-E(i, j)/RT\}$, P_{CO} and P_{O2} are the partial pressures of CO and O_2, $\theta(CO)$ and $\theta(O)$ are the fractional coverages of CO and O, and $\beta(T)$

is the coverage effect of desorption activation energy.

It will be noted that (i) Eq. (3b) includes a temperature-dependent exponential term to account for the effect of coverage on CO desorption (*18*); (ii) the CO and oxygen adsorption sites are assumed to be interchangeable; (iii) the CO_2 formation rate for reaction (1.3) is differentiated from that for reaction (2.3). Equation (3c) contains a square root term of the adatom concentration due to island formation of oxygen adatoms (*23, 24, 40*).

Although Eq. (3c) does not distinguish whether atomic oxygen is adsorbed, as assumed, rather than in oxide form, the oxide does not form below 900 K and is less reactive (*41*). To facilitate model discrimination, Eq. (4b) shows the oxygen adatom concentration term raised to a power of α yet to be determined. A first power corresponds to a LH mechanism for a two-dimensional gas model.

The above rate expressions were employed in a comprehensive mathematical model for the simulation of the transient pulse reaction system under study. The model (*25*) describes the mass conservation of each component of interest, in the gas phase as well as on the catalyst, in the presence of reactions (1.1)–(1.3) during and immediately following the injection of a CO pulse and of reactions (1.1), (1.2), (2.1), and (2.3) during and immediately after the injection of an O_2 pulse. The resulting system of differential equations was solved by computer integration techniques in combination with an optimization program to obtain the best estimates of the kinetic parameters.

Active sites. The maximum amount of CO_2 formed above 400 K during the CO pulse was taken as the molar equivalent of active sites available at each temperature studied. An empirical expression was then derived to relate the active sites as an exponential function of temperature. This expression (Table 3) predicts a maximum CO_2 yield of 0.64 μmol at 350 K, in agreement with the results of the multiple pulse injection experiment shown in Table 1. The empirical correlation of the active sites provides a mathematically simple tool to approximate the multipeak CO desorption characteristics.

The maximum CO_2 formation at 645 K during the CO pulse was 1.25 μmol. Measurements at higher temperatures indicate an asymptotic value of 1.3 μmol, or about 25% of the Pt to be active. Other workers also found only a fraction of the sites on Pt are active (*6, 16*). It may be noted that the maximum oxygen coverage of CO sites is 50% (*2*) and the active β sites represent $\approx$20% of the adsorption sites (*16*).

Parametric sensitivity. Since a quantitative estimate of $k(1.3)$ was unwarranted, this parameter was assigned a sufficiently large value to ensure complete consumption of the preadsorbed oxygen. Initial parametric sensitivity studies showed that a tenfold change in the $k(1.1)$ value resulted in relatively small changes in the estimates for $k(1.2)$, $k(2.1)$, and $k(2.3)$; $k(1.1)$ was then fixed at a value corresponding to a CO sticking coefficient of 0.01, on the basis of the following considerations.

In the low-temperature region of special importance for the study of reaction kinetics, a large CO coverage would be present; the CO sticking coefficient should be sufficiently small (*21–23*). The large coverage predicted supports this choice: For example, at 350 K, after the passage of the O_2 pulse—this presents the initial condition for the subsequent CO pulse—coverages of 0.5 and 0.38 were predicted for $[CO]_{ad}$ and $[O]_{ad}$, respectively. On the other hand, in the high-temperature region, the decrease in CO coverage is compensated for by an increase in $[O]_{ad}$. Hence, the CO sticking coefficient would remain small.

The prediction that a tenfold change in sticking coefficient had a small effect indicates that reaction kinetics are controlling, as should be for the evaluation of the kinetic parameters, and as would be on account of the large sorption flux present under high pressures.

TABLE 2

Predictions of CO_2 Formed by Alternate Models

Temperature (K)/interval (sec)	Observed (μmol)	Model A (μmol)	Model B (μmol)	Model C (μmol)
(1) $CO + [O]_{ad}$				
345/18	0.11	0.14	0.14	0.19
350/18	0.24	0.24	0.28	0.28
350/36	0.39	0.39	0.38	0.37
350/72	0.49	0.49	0.48	0.44
368/18	0.51	0.50	0.67	0.48
(2) $O_2 + [CO]_{ad}$				
345/18	0.17	0.19	0.15	0.21
350/18	0.32	0.32	0.32	0.32
350/36	0.43	0.46	0.43	0.43
350/72	0.51	0.53	0.51	0.51
368/18	0.57	0.57	0.67	0.61
Model Parameter				
Max O_2 coverage		1.0	1.0	0.5
α		0.5	1.0	0.5

Model discrimination. Initial correlations were made on the assumption of the two-dimensional gas LH mechanism; i.e., $\alpha = 1$ and reaction (2.3) would proceed as long as $[CO]_{ad}$ and $]O]_{ad}$ were finite. The model failed to yield reasonable predictions of the observed CO_2 formation. Moreover, it showed CO_2 formation taking place after the passage of the O_2 pulse over the catalyst, which was not observed.

The model was thus revised with the constraint that CO_2 formation by reaction (2.3) would occur only during the passage of O_2 pulse over the catalyst. This implies that at low temperatures (below 400 K), the interior adsorbed CO and oxygen adatoms within their respective island boundaries do not partake the oxidation reaction (*23*), since they are essentially immobile (*38*). At an elevated temperature, CO_2 formation results from oxidation of CO remaining on sites of increasingly stronger bonding strength and hence in relatively immobile clusters near such sites. Thus, the boundary reaction model would apply still. Other workers have also invoked a boundary reaction to account for the oxidation of adsorbed CO (*23, 24, 26*).

However, a model for a boundary reaction at the CO island was tested and abandoned for failure to correlate the experimental data. This point will be discussed in Section V. Further model study shows that $\alpha = 0.5$ (Model A, Table 2) gave the best correlation of the experimental data. This α value was then assumed in the final data correlation. Physically, this α value would indicate the CO_2 formation at the oxygen island boundary to be important, as will be further discussed in Section V.

Most of published O_2 adsorption studies indicate a maximum coverage of 0.5 (*2*). This was tested by model C (Table 2) with an oxygen maximum coverage of 0.5 plus appropriate adjustment for the active sites, to ensure the same maximum CO_2 formation as observed. However, this model yielded a poorer correlation than did Model A based on equal coverage of the active sites by CO and O_2 (*11, 27*).

The procedure for data correlation was as follows: The kinetic parameters were estimated from the data for different pulse intervals at 350 K. Then the activation energies were determined from the data for several runs at temperatures below 390 K.

TABLE 3

Estimates of Kinetic Parameters

Parameter	Value	Remarks
Active sites[a]		
μmol at 350 K	0.64	For catalyst
E (kJ/mol)	4.24	sample studied
CO adsorption		
Sticking coefficient	0.01	Assumed—see
E (kJ/mol)	0.0	text
CO desorption		
k (sec^{-1})	0.164×10^{-6}	350 K
$E(0)$ (kJ/mol)	98-192	See Fig. 5
β (kJ/mol)[b]	27.2	Ref. (*18*)
O_2 adsorption		
Sticking coefficient	0.00025	350 K
E (kJ/mol)	−4.0	Ref. (*28*)
CO_2/O_2 + $[CO]_{ad}$		
k[c] (sec^{-1})	4.27	350 K
E (kJ/mol)	9.8	See Fig. 6

[a] $S_0 = 0.64 * \exp\{510 * (t - 350)/350 * T\}$.

[b] β denotes coverage effect on activation energy for CO desorption as follows: $E = E(0) - \beta * \theta$.

[c] $k = k(2, 3) * (S_0/V_{cat})^{0.5}$.

The complete set of kinetic parameters thus obtained were used to predict the CO formation observed above 400 K. Since no single set of kinetic parameters for CO desorption would succeed, the desorption rate constants were estimated for individual runs above 400 K. Other workers have observed similar sensitivity in correlation of high-temperature rate data (*6, 7*).

Table 3 presents the correlation of the active sites and the best estimates of the other kinetic parameters obtained using Model A. The predicted CO_2 yields are depicted in Figs. 1 and 4 by the dashed lines.

Oxygen adsorption. Low-pressure studies have shown the sticking coefficients of O_2 varying from 0.1 to 10^{-7}, decreasing rapidly with coverage (*30–32*) but moderately with temperature (*31*). The sticking coefficient for O_2 adsorption was thus included in the estimation of the reaction kinetic parameters. A value of 0.00025 was found from the correlation of experimental data at 350 K. This value is consistent with a maximum sticking coefficient of 0.001 on β sites (*32, 16*) and with a sticking coefficient of 0.0005 reported for Pt(*S*)[12(111) × (111)] at a coverage of 0.85 (*31*). It may be noted that the resultant ratio of the sticking coefficients for CO and O_2 (40/1) underlies the well-known phenomenon of CO self-poisoning, due to preferential CO adsorption.

The sticking coefficient at other temperatures was obtained by assuming the apparent activation energy (Table 3) for O_2 adsorption on Pt reported in the literature (*28a, 29*).

CO desorption. As shown in Fig. 5, the desorption rate constants found are in agreement with those from low-pressure studies of unsupported Pt. For comparison, published desorption rates for Pt[111] (*28a*) were extrapolated to low temperatures. Another study of Pt[111] (*33*) found a desorption activation energy of 125 kJ/mol.

To ascertain the importance of the exponential term for the CO coverage dependence of the heat of adsorption, correlation studies were made in the absence of such a

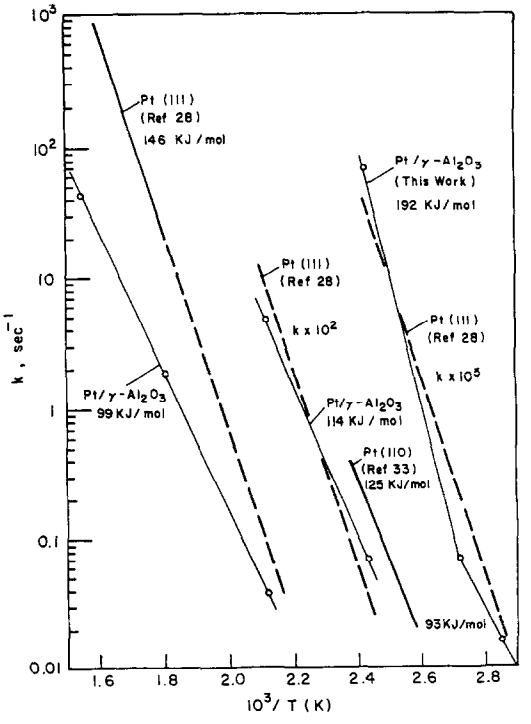

FIG. 5. Rate constant of CO desorption.

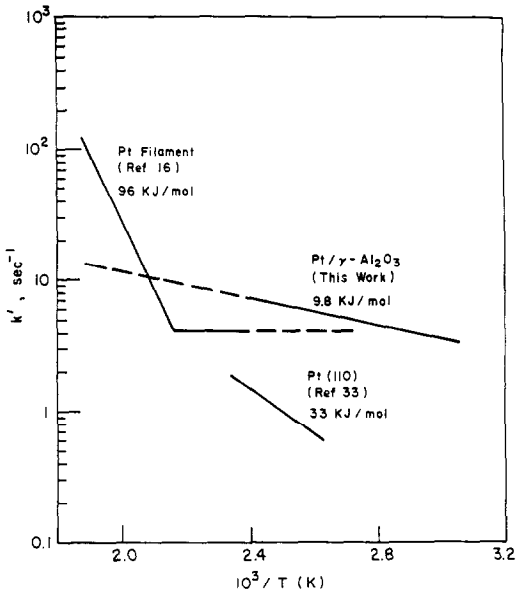

FIG. 6. Rate constant of CO_2 formation/O_2(g) + $[CO]_{ad}$.

coverage effect. The results confirmed that such a term was necessary (*7*) and that the effect of coverage on CO desorption was essentially the same as reported in the literature (*18*).

The desorption rate constant found in the present study indicate at least two desorption peaks, namely, one peak at a temperature below 360 K and another at about 410 K, as indicated by a change in the activation energy (Fig. 5). As shown in Fig. 4B, CO_2 formation at 368 K during the CO pulse appears to pass through a maximum at a pulse interval of 36–72 sec. This reflects a saddle point in the desorption characteristics due to two adjacent peaks. The activation energies found in our study (93–114 kJ/mol, excepting the high value for the peak near 410 K) are in good agreement with published studies (*18, 21, 24, 28b*), showing activation energies of 100–150 kJ/mol.

The desorption rate constants at 410 K was confirmed by a separate desorption study. Due to slow desorption, the desorption rate constants at lower temperatures could not be determined with accuracy. The high-activation energy (192 kJ/mol) found for the desorption peak near 410 K probably represents an artifact. Namely, the simplified desorption model (based on an empirical correlation of active sites with temperature) fails to give an exact account of the contribution due to the tail(s) of the leading peak(s) to the front end of the peak near 410 K. The simplified CO desorption model probably results also in the trend of activation energy decreasing with temperature above 410 K.

It also should be noted that an increased step concentration of supported metal and strong metal–support interactions will increase the bonding strength (*12, 31, 34, 35*). The high activation energy found for the desorption peak near 410 K may be due also to the surface morphology of the supported Pt. The decreasing trend of desorption activation energy at temperatures above 400 K may be due also to a surface reconstruct from the cyclic redox reaction at increasing high temperatures (*32, 44*).

Surface reaction. Figure 6 shows the reaction rate constants found for the O_2(g) + $[CO]_{ad}$ system with a linear extrapolation to high temperatures indicated by a dotted line. The low activation energy of 10 kJ/mol (Fig. 6) indicates that the oxidation at the island perimeter involves a facile reaction, as expected from the observation that the reaction between $[O]_{ad}$ and $[CO]_d$ in proximity is fast (*2, 20*).

It is noteworthy that the results of the present study agree with the rate constant for a Pt filament within a factor of $\approx$2 and with that for Pt[110] within a factor of 10, despite the wide range of pressures employed. Since the supported metal would exhibit a polycrystalline surface rather than a well-defined crystalline plane, the activity of supported Pt should be similar to that of the Pt filament rather than to that of the Pt[110].

V. REACTION MECHANISMS

CO_2 Formation from O_2(g) + $[CO]_{ad}$. A LH pathway is commonly assumed for the

oxidation of preadsorbed CO with oxygen adatoms, since the prerequisite for rupture of the strong O=O bond precludes the involvement of oxygen in a weakly adsorbed precursor state (*28a, 30, 31*) or adsorbed molecular oxygen. As shown in Fig. 6, the involvement of an ER reaction mechanism may not be ruled out. It is thus important to reconcile the LH reaction mechanism reported in other studies with our results suggesting a modified ER pathway, i.e., involvement of weakly adsorbed CO and a small activation energy.

First, we note that for the Pt filament study (Fig. 6), the CO_2 evolution at temperatures above 500 K was found to exceed the oxygen sorption rate (*16*), showing a significant contribution due to diffusion. Thus, the break in the temperature dependence of the rate constant reflects a dominant diffusion flux with increasing temperature. The nature of the diffusion involved will be discussed later.

The commonly assumed two-dimensional gas (TDG) LH model presumes unlimited diffusion of the adsorbates and hence is inadequate in view of the formation of separate adsorbate islands on the metal (*23, 40*). Thus, the oxidation reaction rate would be proportional to the product of the adsorbate concentrations, each raised to a power of 0.5. In our study we have found $\alpha = 0.5$ indeed but retained the linear relationship with adsorbed CO in view of its mobility (*2, 21, 22, 28a*). It is thus necessary to examine the kinetic implications of readsorption and diffusion underlying the CO mobility.

In our kinetic model CO readsorption is accounted for in the CO balance through the adsorption and desorption steps. However, surface diffusion, an activated process, has not been explicitly accounted for and its effect will emerge as an activation energy unrelated to the intrinsic reaction kinetics. This is analogous to the well-known pore diffusion effect, except that pore diffusion, a nonactivated process, results in a lower apparent activation energy. Due to its high activation energy (*38a, 38b*), surface diffusion results in a higher apparent activation energy. Thus, high activation energy fails here as the criterion for a LH pathway.

In our study pore diffusion is not important, the Thiele's modulus being less than 1, and the activation energy found is not tinted by bulk-gas-phase transport. Moreover, the sorption flux at a pressure of 1–2 kPa is seven orders of magnitude greater than that under low pressures of $\approx 10^{-4}$ Pa. As indicated by the diffusion-controlled rate for the Pt filament (Fig. 6), the surface diffusion rate over the temperatures studied is at most two orders of magnitude larger than the sorption rate at 10^{-4} Pa. Hence, diffusion of the adsorbate from the reactant in the injected pulse is unimportant.

(*A*) *Proposed reaction mechanism.* Conceivably, the boundary reaction may involve either oxygen adatoms near the CO island or adsorbed CO near the oxygen island being formed during the oxygen pulse. If the boundary reaction at the CO island involving oxygen adatoms formed *in situ* dominates, the CO_2 formation will vary with the square root of CO coverage. However, such a reaction model did not yield good correlation of the experimental data whereas a kinetic model based on a boundary reaction near the oxygen island ($\alpha = 0.5$) did. Spatial requirement considerations (e.g., presence of paired adjacent vacant sites) (*45*) would suggest that the boundary reaction at the CO island may be limited and unimportant. Thus, our results show CO_2 formation to result from the boundary reaction at the oxygen island.

The observation that CO_2 formation occurred only during the oxygen pulse results from CO diffusion confining the reaction within a limited distance from island boundary at low temperatures, where readsorption is unimportant. During the pulse the oxygen maintains a supply of adatoms within this perimeter whereas afterward CO_2 formation stops as the remaining oxygen adatoms are beyond the effective zone.

On the other hand, during the subsequent CO pulse the remaining oxygen will be efficiently removed by the intrinsic fast oxidation as CO diffusion is unimportant during a CO pulse.

It may be noted that diffusion suggests mobility which in turn means relaxation of the metal CO bond. Conceivably, the CO island may consist of an active center (defects/steps) with a strong bonding strength surrounded by weaker adsorption sites with bonding energies decreasing in proportion to the distance from the center, while the distribution of CO on the island is dictated by a dynamic equilibrium, in the sense that with increasing temperature the equilibrium will favor the adsorption on the outer weaker sites. The concept of such a dynamic adsorbate distribution is not incompatible with the intrinsic heterogeneity of adsorption sites (*26, 16–19*) and may even underlie the diffusion mechanism.

The activation energy found in our study is significantly smaller than that for CO diffusion (40–60 kJ/mol) (*38a*), indicating that CO diffusion is not controlling during the oxygen pulse, for the reasons noted above. Moreover, it is closer to the energy barrier for diffusion of physically adsorbed CO ($\approx$4 kJ/mol) (*38a*) than to the metal CO bond strength (74–138 kJ/mol) (*2, 41*). It follows that the boundary reaction involves weakly adsorbed CO.

It may be noted that at elevated temperatures oxygen diffusion by virtue of its high activation energy (*38b*) may play a role under low pressures but not in our study. At low temperatures CO diffusion will be important, as evidenced by predicted CO_2 being higher than observed at 330 K (Table 2). Thus, the rate constant of our study may be extrapolated to high temperatures but should not be extrapolated to lower temperatures (Fig. 6).

(*B*) *Comparison with other studies.* All kinetic studies in the literature assume a TDG model for $[CO]_{ad}$ and most of them also assume a TDG model for oxygen adatoms. Then, the activation energy found in other studies, especially under low pressures, may reflect diffusion-disguised kinetics and needs to be examined. For convenience, we shall denote the commonly assumed model based on complete mixing of both adsorbates as a TDG LH model and a kinetic model assuming a TDG for CO surrounding oxygen islands as a TDG model.

First, we note that when experimental data were analyzed by a TDG LH model, a low-pressure study (*45*) showed an activation energy (6 kJ/mol) comparable to ours, indicating that CO diffusion is not controlling under the temperatures studied. Moreover, the reported rate constants (0.4 to 1.4 sec^{-1} over 300–500 K) are in reasonable agreement with ours, especially in view of the fact that the cited study assumed all adsorption sites being active and would yield low estimates of the rate constant at the active sites. There is thus general agreement between our study and the low-pressure study cited.

However, molecular beam studies (*36, 37*), based on a TDG LH model, yielded an apparent activation energy of $\approx$100 kJ/mol. Since these studies were made at temperatures above $\approx$500 K, oxygen diffusion might be important and the observed activation energy would provide no conclusive evidence for a LH pathway. The fact that the observed activation energy is comparable to the energy barrier for oxygen diffusion (110 kJ/mol) (*38b*) strongly suggests that it reflects oxygen diffusion-disguised kinetics.

As noted earlier, mass balance consideration shows that the high activation energy found in the Pt filament study (Fig. 6) would reflect diffusion-disguised kinetics, as also evidenced by the activation energy found at temperatures above 500 K being comparable to the energy barrier for oxygen diffusion.

On the other hand, the rate constants of Ref. (*33*) (Fig. 6) were based on a TDG LH model which neglected CO readsorption. Since oxygen or CO diffusion is not ex-

pected to be important at the temperatures studied, the activation energy found seems to represent an artifact due to the omission of CO readsorption.[1] Such omission would cause a false depletion of adsorbed CO, due to desorption (an activated process), and hence the rate constant had to be enhanced, in the data correlation, in order to fit the observed CO_2 yield.

The above observations show that the proposed modified ER reaction mechanism is consistent with the low-pressure studies when the apparent activation energy due to diffusion-disguised kinetics or omission of readsorption has been accounted for.

CO_2 formation from $CO(g) + [O]_{ad}$. The data for this reaction show significant features of the kinetics indicating the involvement of weakly adsorbed CO in a facile reaction on oxygen island boundary.

First, even at a low temperature of 350 K the CO_2 evolution precedes the CO breakthrough (Fig. 3B). Moreover, multiple-pulse experiments have shown that one CO pulse is sufficient to remove all the oxygen adsorbed on the catalyst (Table 1). The CO_2 formation near the oxygen island boundary is thus very fast indeed, as has been noted in the titration of preadsorbed oxygen with CO (*21, 22, 45*).

Second, the CO_2 formation rate is independent of temperature (Fig. 2B), as has also been observed in other low-pressure studies (*2, 17, 36, 42, 43, 45*). This implies an oxidation reaction with a small energy barrier and the involvement of weakly adsorbed CO. It may be noted that a small energy barrier is not, whereas a large activation energy is, incongruous with a facile reaction.

It also may be noted that several studies have indicated the involvement of physically adsorbed CO in a mobile precursor state (*22, 42, 43*) and that the weakly adsorbed precursor state has a finite residence time (*14*) (in order for the reaction to take place).

The low-pressure studies of $CO_2/O_2(g) + [CO]$ discussed above show oxygen diffusion-disguised kinetics at elevated temperatures. Such a diffusion effect is unimportant in our study under high pressures because the oxygen diffusion would be overtaken by the overwhelming CO sorption flux prevalent. In addition, whereas $CO_2/O_2(g) + [CO]_{ad}$ in our study will depend on CO diffusion as well as dissociative adsorption of oxygen at low temperatures, $CO_2/CO(g) + [O]_{ad}$ does not.

Comparison with other studies. As noted above, our results are in agreement with a number of low-pressure studies indicating temperature independence. However, molecular beam studies have reported activation energies of 40–50 kJ/mol as evidence for a LH pathway (*37, 39*). Due to the inadequacy of the TDG LH model assumed, the observed activation energy does not ensure a LH pathway sans a detailed analysis based on mass conservation principle.

In absence of such analysis, we note that the boundary reaction model would predict a CO diffusion effect at low temperatures and that at high temperatures oxygen, not CO, diffusion will be important as noted for $CO_2/O_2(g) + [CO]_{ad}$ under low pressures. The predicted CO diffusion effect is consistent with reported titration of preadsorbed oxygen with CO at low temperatures ($\approx$350 K) (*21, 22*) and CO_2 formation from adsorbed CO in the presence of preadsorbed oxygen (*23*).

Since the activated energy found in the CO beam study below $\approx$300 K (50 kJ/mol/mol) (*37*) is of the same magnitude as the energy barrier for the diffusion of CO (40–60 kJ/mol) (*38a*) and quite different from the metal–CO bonding energy (74–138 kJ/mol) (*2, 41*), we interpret it as to reflect CO diffusion-disguised kinetics.

However, a similar activation energy (40 kJ/mol) was found in the CO beam study above 500 K (*39*). The discrepancy with expectation is reconciled by the following ob-

[1] It may be noted that the omission of CO readsorption plus assumption of all adsorption sites being active underlies the failure to fit the observed induction period (*33*).

servations. First, molecular beam studies seem to show a beam-dependent effect, i.e., a CO diffusion effect with CO beam (*39*) and oxygen diffusion-disguised kinetics with O_2 beam (*37*). Second, another beam study (*36*), based on mass spectroscopy instead of CO_2 evolution phase shift, showed CO_2 formation independent of temperature (300–700 K), i.e., negligible activation energy, in agreement with the other studies cited as well as with ours.

Thus the phase shift technique appears to measure beam-dependent diffusion-disguised kinetics. While it is beyond the scope of this study to ascertain the underlying factors,[2] it suffices to note that CO diffusion for $CO_2/CO(g) + [O]_{ad}$ is unimportant under high pressures and that the mass spectroscopy beam study showed an activation energy of 92 kJ/mol from the oxygen beam experiment, indicating oxygen diffusion-disguised kinetics for $CO_2/O_2(g) + [CO]_{ad}$ under low pressures to be instrument independent and hence real.

The activation energy obtained by the CO beam study based on the CO_2 evolution phase shift at temperatures above 500 K (*39*) appears to show an instrument-related diffusion-disguised kinetics and remains to be confirmed. It also may be noted that an activation energy over 130 kJ/mol for $CO_2/CO(g) + [O]_{ad}$ has been reported (*45*). Though such a high activation energy is possible (such as due to boundary-free diffusion of oxygen) (*38b*), it was derived by a simplified TDG model based on incompatible assumptions (*46*) and hence may be discounted.

With the above two instances excepted, the proposed modified ER reaction mechanism is compatible with low-pressure studies of $CO_2/CO(g) + [O]_{ad}$, as in the case of $CO_2/O_2(g) + [CO]_{ad}$, when diffusion-disguised kinetics are accounted for. Due to limited time resolution (20 msec) of the data acquisition system and relatively slow instruments used, our study of $CO_2/CO(g) + [O]_{ad}$ has yielded qualitative, albeit diffusion-free, kinetics. A quantitative confirmation will have to be obtained with sufficiently fast data acquisition and instruments.

[2] The phase shift technique might have detected CO_2 formed within the beam umbra from oxidation of the mobile CO plus the small angle deflections of CO desorbed from step/defect sites (*28a*), while mass spectroscopy would have sampled CO_2 formation on a macroscale.

VI. CONCLUDING REMARKS

Adsorbate diffusion plays an important role in catalysis in general, and in low pressure study in particular, since a catalyzed reaction will involve diffusion of adsorbed species to the active center either as a reactive island boundary or as an active site. As the reaction taking place at the active center is, as should be, very fast whereas the adsorption rate is small (*26*, *16*), a rigorous study of low-pressure kinetics requires an exact account of the transport of the adsorbates. The shortcomings of the commonly assumed two-dimensional gas LH model discussed in the preceding section apply in principle to catalyzed reactions in general.

In principle, the kinetic parameters found under low pressures can be used to predict high-pressure kinetics; however, this entails a complete knowledge of the intrinsic kinetics and of the active sites. Until then, kinetic studies under high pressures will be both necessary and valuable.

In summary, CO_2 formation from $O_2(g) + [CO]_{ad}$ as well as from $CO(g) + [O]_{ad}$ involves a boundary reaction at the oxygen island with an energy barrier of ≈ 10 kJ/mol, indicating the involvement of mobile weakly adsorbed CO. The boundary reaction model, in the presence or absence of diffusion, provides a unified view of the reaction kinetics observed under low, as well as under high, pressures, when diffusion-disguised kinetics are properly accounted for.

ACKNOWLEDGMENTS

The authors are indebted to M. Shelef and H. S. Gandhi for their encouragement during this work and

to D. Lewis and M. Rokosz for their assistance in catalyst characterization.

REFERENCES

1. Langmuir, I., *Trans. Faraday Soc.* **17,** 321 (1922).
2. Engel, T., and Ertl, G., "Advances in Catalysis" (D. D. Eley, P. W. Sellwood, and P. B. Weisz, Eds.), Vol. 17, p. 1. Academic Press, New York, 1979.
3. Creighton, J. R., and White, J. M., *in* "Catalysis Under Transient Conditions" (A. T. Bell and L. L. Hegedus, Eds.), ACS Symp. Ser., Vol. 178, p. 23. American Chemical Society, Washington, DC, 1982.
4. Razon, L. F., and Schmitz, R. A., *Catal. Rev. Sci. Eng.* **28**(1), 89 (1986).
5. Yeates, R. C., Turner, J. C., Gellman, A. J., and Somarai, G. A., *Surf. Sci.* **149,** 175 (1985).
6. Herz, R., and Marin, S. P., *J. Catal.* **65,** 281 (1980).
7. Cho, B. K., *Chem. Eng. Commun.* **47,** 201 (1986).
8. Haaland, D. M., and Williams, F. L., *J. Catal.* **76,** 450 (1982).
9. Barshad, Y., Zhou, X., and Gulari, E., *J. Catal.* **94,** 128 (1985).
10. Cameron, P., Scott, R. P., and Watts, P., *J. Chem. Phys., Faraday Trans.* **1,** 82, 1389 (1986).
11. Dwyer, S. M., and Bennett, C. O., *J. Catal.*, **95,** 275 (1982).
12. Yao, H. C., Sieg, W., and Plummer, H. K., *J. Catal.* **59,** 365 (1979).
13. Su, E. C., and Rothschild, W. G., *J. Catal.* **99,** 506 (1986).
14. Kisliuk, P. J., *J. Phys. Chem. Solids* **3,** 95 (1957).
15. Rothschild, W. G., and Su, E. C., *Bull. Amer. Phys. Soc.* **29,** 348 (1984).
16. Winterbottom, W. L., *Surf. Sci.* **36,** 205 (1973).
17. Nishiyama, Y., and Wise, H., *J. Catal.* **32,** 50 (1974).
18. McCabe, R. W., and Schmidt, L. D., *Surf. Sci.* **66,** 101 (1977).
19. Derry, G. N., and Ross, P. N., *Surf. Sci.* **140,** 165 (1984).
20. Heyne, H., and Thompkins, F. C., *Proc. R. Soc. London A* **292,** 460 (1966).
21. Behm, R. J., Thiel, P. A., and Norton, P. R., and Binder, P. E., *Surf. Sci.* **147,** 143 (1984).
22. Golchet, A., and White, J. M., *J. Catal.* **53,** 266 (1978).
23. Gland, J. L., and Kollin, E. B., *J. Chem. Phys.* **78,** 963 (1983).
24. Sarkany, J., Bartok, M., and Gonalez, R. P., *J. Catal.* **81,** 347 (1983).
25. Su, E. C., Rothschild, W. G., and Yao, H. C., Tech. Report 87-223, Eng. and Res. Staff, Ford Motor Co., Dearborn, MI 48121.
26. Matsushima, T., *Surf. Sci.* **79,** 63 (1979).
27. Ducros, R., and Merrill, R. P., *Surf. Sci.* **55,** 227 (1976).
28. Campbell, C. T., Ertl, G., Kuipers, H., and Segner, J., (a) *Surf. Sci.* **107,** 207 (1981); (b) *Surf. Sci.* **107,** 220 (1981).
29. Gland, J. L., *Surf. Sci.* **93,** 487 (1980).
30. Bonzel, H. P., and Ku, R., *Surf. Sci.* **40,** 85 (1973).
31. Gland, J. L., and Korchak, V. N., *Surf. Sci.* **75,** 733 (1978).
32. Norton, P. R., Griffiths, K., and Binder, P. E., *Surf. Sci.* **138,** 125 (1984).
33. Bonzel, H. P., and Burton, J. J., *Surf. Sci.* **52,** 223 (1975).
34. Hopster, H., Ibach, H., and Cosma, G., *J. Catal.* **46,** 37 (1977).
35. Rothschild, W. G., Yao, H. C., and Plummer, H. K., *Langmuir* **2,** 588 (1986).
36. Pacia, N., Cassuto, A., Pentenero, A., and Weber, B., *J. Catal.* **41,** 455 (1976).
37. Campbell, C. T., Ertl, G., Kuipers, H., and Segner, J., *J. Chem. Phys.* **73,** 5862 (1980).
38. Lewis, R., and Gomer, R., (a) *Nuovo Cimento Suppl.* **5,** 506 (1967); (b) *Surf. Sci.* **12,** 157 (1968).
39. Fair, J. A., and Madix, R. J., *J. Chem. Phys.* **73,** 3186 (1980).
40. Gland, J. L., Sexton, B. A., and Fisher, G. B., *Surf. Sci.* **95,** 587 (1980).
41. Herz, R. K., and McCready, D. F., *J. Catal.* **81,** 358 (1983).
42. Matsushima, T., Almy, D. B., and White, J. M., *Surf. Sci.* **67,** 89 (1977).
43. Alnot, M., Fusy, J., and Cassuto, A., *Surf. Sci.* **57,** 651 (1976).
44. Griffiths, K., Jackman, T. E., Davis, J. A., and Norton, P. R., *Surf. Sci.* **138,** 113 (1984).
45. Barteau, M. A., Ko, E. J., and Madix, R. J., *Surf. Sci.* **104,** 161 (1981).
46. Bechtold, E., *Surf. Sci.* **115,** L125 (1982).